

Monomeric, trimeric, and tetrameric transition metal complexes (Mn, Fe, Co) containing *N,N*-bis(2-pyridylmethyl)-2-aminoethanol/-ate: preparation, crystal structure, molecular magnetism and oxidation catalysis†Jong Won Shin,^a Sankara Rao Rowthu,^a Min Young Hyun,^b Young Joo Song,^b Cheal Kim,^{*b} Bong Gon Kim^c and Kil Sik Min^{*a}

Received 7th January 2011, Accepted 25th March 2011

DOI: 10.1039/c1dt10028a

The reaction of *N,N*-bis(2-pyridylmethyl)-2-aminoethanol (bpaeOH), NaSCN/NaN₃, and metal (M) ions [M = Mn(II), Fe(II/III), Co(II)] in MeOH, leads to the isolation of a series of monomeric, trimeric, and tetrameric metal complexes, namely [Mn(bpaeOH)(NCS)₂] (**1**), [Mn(bpaeO)(N₃)₂] (**2**), [Fe(bpaeOH)(NCS)₂] (**3**), [Fe₄(bpaeO)₂(CH₃O)₂(N₃)₈] (**4**), [Co(bpaeOH)(NCS)₂] (**5**), and [Co₃(bpaeO)₂(NO₃)(N₃)₄](NO₃) (**6**). These compounds have been investigated by single crystal X-ray diffraction and magnetochemistry. In complex **1** the Mn(II) is bonded to one bpaeOH and two thiocyanate ions, while in complex **2** it is coordinated to a deprotonated bpaeO⁻ and two azide ions. The oxidation states of manganese ions are 2+ for **1** and 3+ for **2**, respectively, indicating that the different oxidation states depend on the type of binding anions. The structures of monomeric iron(II) and cobalt(II) complexes **3** and **5** with two thiocyanate ions are isomorphous to that of **1**. Compounds **1**, **2**, **3**, and **5** exhibit high-spin states in the temperature range 5 to 300 K. **4** contains two different iron(III) ions in an asymmetric unit, one is coordinated to a deprotonated bpaeO⁻, an azide ion, and a methoxy group, and the other is bonded to three azide ions and two oxygens from bpaeO⁻ and a methoxy group. Two independent iron(III) ions in **4** form a tetranuclear complex by symmetry. **4** displays both ferromagnetic and antiferromagnetic couplings ($J = 9.8$ and -14.3 cm⁻¹) between the iron(III) ions. **6** is a mixed-valence trinuclear cobalt complex, which is formulated as Co^{III}($S = 0$)–Co^{II}($S = 3/2$)–Co^{III}($S = 0$). The effective magnetic moment at room temperature corresponds to the high-spin cobalt(II) ion ($-4.27 \mu_B$). Interestingly, **6** showed efficient catalytic activities toward various olefins and alcohols with modest to excellent yields, and it has been proposed that a high-valent Co^V-oxo species might be responsible for oxygen atom transfer in the olefin epoxidation and alcohol oxidation reactions.

Introduction

The design and preparation of mono- and polynuclear transition metal complexes has enabled the understanding and development of molecule-based magnetic materials and the structural elucidation of metalloenzymes in biological systems, as well as the development of catalysts for hydrocarbon oxidations.¹ It has been recognized that the metal centers and the binding ligands as anions or capping molecules may play important roles in the formation of desirable compounds, due to the molecular shape, charge,

and size.² Recently, a zigzag tetranuclear iron(III) complex with bridged azide and methoxy ions and *N,N*-bis(2-pyridylmethyl)-2-aminoethanolate ions has been reported.³ The complex has shown interesting magnetic properties, indicative of both ferromagnetic and antiferromagnetic interactions. The tetradentate *N,N*-bis(2-pyridylmethyl)-2-aminoethanolate (bpaeO⁻) is a multifunctional ligand, in which it has a potential N₃ donor as bis(picoly)amine and an oxygen atom acting as proton donor/acceptor. As relating to bpaeO⁻, studies on the metal complexes with organic derivatives including *N,N*-bis(2-pyridylmethyl)-2-aminoethanolate moiety have been performed with objectives such as sequence-specific cleavage of DNA, synthesis of biodegradable polymers, and the development of quadruplex DNA binders.⁴ Furthermore, the tetradentate ligand as a capping molecule has been used in the formation of a bis(μ -alkoxo)-bridged dinuclear iron(III) complex as a biomimetic model for the intradiol-cleaving dioxygenase enzymes and the synthesis of oxorhenium(V) and copper(II) complexes for mechanistic studies and cleaving an activated phosphate diester.⁵

^aDepartment of Chemistry Graduate School, Kyungpook National University, Daegu, 702-701, Republic of Korea. E-mail: minks@knu.ac.kr

^bDepartment of Fine Chemistry, Seoul National University of Science and Technology, Seoul, 139-743, Republic of Korea. E-mail: chealkim@snut.ac.kr

^cDepartment of Chemistry Education, Gyeongsang National University, Jinju, 660-701, Republic of Korea

† Electronic supplementary information (ESI) available. CCDC reference numbers 749014, 806664–806668. For ESI and crystallographic data in CIF or other electronic format see DOI: 10.1039/c1dt10028a

The versatile azide ion for dimers, clusters, and polymers exhibiting significant magnetic properties such as ferro- and antiferromagnetic interactions has been extensively used because it may induce interesting magnetic couplings by two different bonding modes, *i.e.* end-on (μ -1,1, ferromagnetic) and end-to-end (μ -1,3, antiferromagnetic).⁶ Additionally, mixed-valence compounds have been studied in relation to the characterization of magnetic exchange interactions and valence tautomerism.⁷ For example, the cobalt-based $[(\text{TPyA})\text{Co}^{\text{III}}(\text{DBQ}^{3-})\text{Co}^{\text{III}}(\text{TPyA})](\text{BF}_4)_3$ complex is identified as $[(\text{TPyA})\text{Co}^{\text{II}}(\text{DBQ}^{2-})\text{Co}^{\text{III}}(\text{TPyA})](\text{BF}_4)_3$ over room temperature [TPyA = tris(2-pyridylmethyl)amine; $\text{DBQ}^{3-} = 2,5\text{-di-}i\text{-tert-butyl-3,6-dihydroxy-1,4-benzoquinonate}$].⁸ The mixed-valence cobalt compound is obtained through electron transfer depending on the temperature. Likewise, such compounds can potentially also be used as catalysts for oxidation.

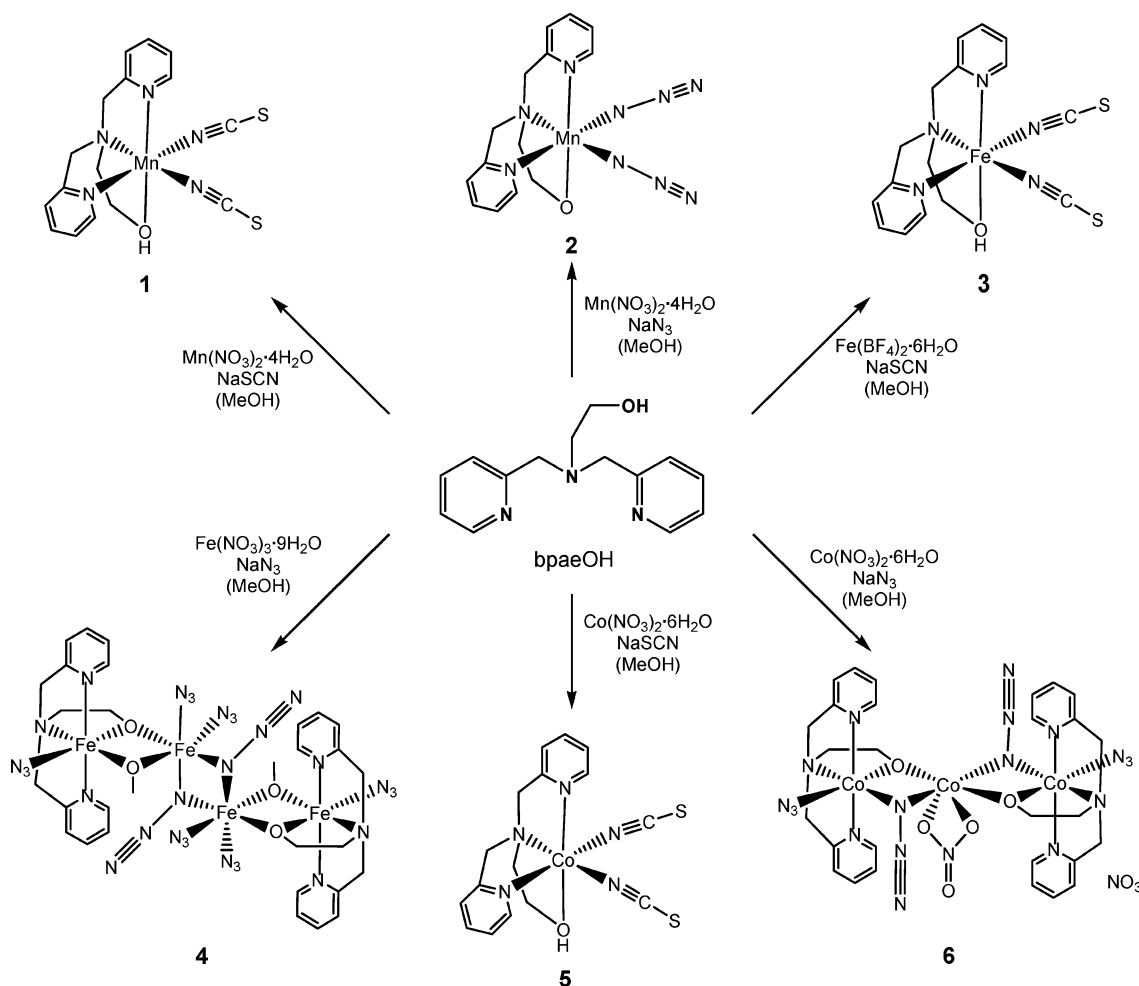
In a continuation of our previous work on the tetranuclear Fe(III) complex with *N,N*-bis(2-pyridylmethyl)-2-aminoethanol and azide ions, we have prepared a series of novel transition metal complexes with Mn/Fe/Co and bpaeOH as well as $\text{NCS}^-/\text{N}_3^-$ ions; $[\text{Mn}(\text{bpaeOH})(\text{NCS})_2]$ (**1**), $[\text{Mn}(\text{bpaeO})(\text{N}_3)_2]$ (**2**), $[\text{Fe}(\text{bpaeOH})(\text{NCS})_2]$ (**3**), $[\text{Fe}_4(\text{bpaeO})_2(\text{CH}_3\text{O})_2(\text{N}_3)_8]$ (**4**), $[\text{Co}(\text{bpaeOH})(\text{NCS})_2]$ (**5**), and $[\text{Co}_3(\text{bpaeO})_2(\text{NO}_3)(\text{N}_3)_4](\text{NO}_3)$ (**6**) (Scheme 1). For comparison to the azide ion, the thiocyanate (NCS^-) ion which has various bonding modes (end-on, end-to-

end, terminal, bridging)⁹ was used to obtain transition metal complexes (**1**, **3**, **5**). It has been reported that the azide (N_3^-) ion is a stronger oxidizing agent than the thiocyanate (NCS^-) ion in aqueous and mixed medium.¹⁰ Monomeric metal(II) octahedral complexes (**1**, **3**, **5**) are formed using the NCS^- ion, while polynuclear complexes (**4**, **6**) including the mononuclear Mn(III) compound **2** are obtained using the N_3^- ion. Herein we report the synthesis, structure and magnetic properties of **1–6**. In addition, the catalytic activities toward hydrocarbon oxidation of mixed-valence complex **6** will be also described.

Experimental

General

All chemicals used in the synthesis and oxidation reactions were of reagent grade and used without further purification. *N,N*-bis(2-pyridylmethyl)-2-aminoethanol (bpaeOH) was prepared according to the literature procedure.¹¹ UV-Vis absorption spectra were recorded with a SCINCO S-2100 spectrophotometer. Infrared spectra were recorded with a Thermo Fisher Scientific IR200 spectrophotometer ($\pm 1 \text{ cm}^{-1}$) using KBr disks. Elemental analyses were carried out using a Fisons/Carlo Erba EA1108 instrument. Magnetic susceptibilities were measured in an applied field of



Scheme 1 Schematic presentation of the formation of transition metal complexes 1–6.

5000 Oe between 2 or 5 and 300 K on a Quantum Design MPMS superconducting quantum interference device (SQUID) magnetometer. Diamagnetic corrections were made [226.8 (1), 258.3 (2), 219.3 (3), 724.8 (4), 224.2 (5), and 542.6×10^{-6} (6) emu mol⁻¹] by using Pascal's constants. Susceptibility data of 1–6 were simulated with the julX program package for magnetic models.¹² The zero-field Mössbauer spectrum of 4 was recorded at room temperature. The spectrometer was calibrated by collecting the Mössbauer spectra of a standard α -Fe foil at room temperature. The Mössbauer parameters were obtained by a least-square fitting program assuming Lorentzian line shapes. Product analysis for the oxidation reaction was performed on either a Hewlett–Packard 5890 II Plus gas chromatograph interfaced with a Hewlett–Packard Model 5989B mass spectrometer or a Donam Systems 6200 gas chromatograph equipped with an FID detector using a 30-m capillary column (Hewlett–Packard, HP-1, HP-5, and Ultra 2).

Syntheses of compounds

[Mn(bpaeOH)(NCS)₂] (1). To an MeOH solution (5 mL) of Mn(NO₃)₂·4H₂O (104 mg, 0.41 mmol) was added an MeOH solution (5 mL) of bpaeOH (100 mg, 0.41 mmol) and an MeOH solution (5 mL) of sodium thiocyanate (67 mg, 0.82 mmol). The mixture was stirred for 1 h at room temperature. The resulting solution was allowed to stand at ambient temperature until pale yellow crystals had formed, which were collected by filtration, washed with diethyl ether, and air dried (yield: 107 mg, 63%). Anal. calcd for C₁₆H₁₇MnN₃OS₂: C, 46.37; H, 4.13; N, 16.90; S, 15.48. Found: C, 46.34; H, 4.13; N, 16.92; S, 14.90. FT–IR (KBr, cm⁻¹): $\nu(\text{OH})$ 3423, 3253; $\nu(\text{SCN}^-)$ 2068, 2056; $\nu(\text{C–H})$ 2962, 2899; $\nu(\text{C–O})$ 1060, 1016; $\nu(\text{C–N})$ 1603; $\nu(\text{C–C})$ 1440.

[Mn(bpaeO)(N₃)₂] (2). To an MeOH solution (5 mL) of Mn(NO₃)₂·4H₂O (104 mg, 0.41 mmol) was added an MeOH solution (5 mL) of bpaeOH (100 mg, 0.41 mmol) and an MeOH solution (5 mL) of sodium azide (54 mg, 0.82 mmol). The resulting solution was stirred for 1 h at room temperature and then allowed to stand in a refrigerator for 3 days. Dark gray crystals were formed and collected by filtration and washed with cold methanol and diethyl ether and dried in air (yield: 70 mg, 45%). Anal. calcd for C₁₄H₁₆MnN₆O: C, 44.11; H, 4.23; N, 33.06. Found: C, 43.93; H, 4.21; N, 32.69. FT–IR (KBr, cm⁻¹): $\nu(\text{N}_3^-)$ 2066, 2044; $\nu(\text{C–H})$ 3052, 2957, 2837; $\nu(\text{C–O})$ 1062, 1040; $\nu(\text{C–N})$ 1601, 1286; $\nu(\text{C–C})$ 1444.

[Fe(bpaeOH)(NCS)₂] (3). To an MeOH solution (4 mL) of Fe(BF₄)₂·6H₂O (69 mg, 0.21 mmol) was added an MeOH solution (4 mL) of bpaeOH (50 mg, 0.21 mmol) and an MeOH solution (4 mL) of sodium thiocyanate (33 mg, 0.41 mmol). The mixture was stirred for 1 h at room temperature. The color of the mixture turned orange–yellow and then orange–yellow solid formed. The solid was collected by filtration and washed with methanol and diethyl ether and dried in air (yield: 38 mg, 44%). Orange–yellow crystals of 3 suitable for X-ray crystal analysis were obtained by diffusion of diethyl ether into the MeOH solution of 3. Anal. calcd for C₁₆H₁₉FeN₅O₂S₂: C, 44.35; H, 4.42; N, 16.16; S, 14.80. Found: C, 44.21; H, 3.90; N, 16.18; S, 14.55. FT–IR (KBr, cm⁻¹): $\nu(\text{OH})$

3426, 3248; $\nu(\text{SCN}^-)$ 2077, 2059; $\nu(\text{C–H})$ 2924; $\nu(\text{C–O})$ 1052, 1018; $\nu(\text{C–N})$ 1604, 1346, 1320, 1290; $\nu(\text{C–C})$ 1442.

[Fe₂(bpaeO)₂(CH₃O)₂(N₃)₈] (4). To an MeOH solution (10 mL) of Fe(NO₃)₃·9H₂O (994 mg, 2.46 mmol) was added an MeOH solution (10 mL) of *N,N*-bis(2-pyridylmethyl)-2-aminoethanol (bpaeOH, 300 mg, 1.23 mmol) and an MeOH solution (10 mL) of sodium azide (560 mg, 8.61 mmol). The mixture was stirred for 1 h at room temperature. The color turned reddish–brown and then reddish–brown solid formed. The precipitate was collected by filtration and washed with methanol and diethyl ether and dried in air (yield: 524 mg, 77%). Reddish–brown needle-shaped crystals of 4 suitable for X-ray crystal analysis were obtained by layering of the MeOH solution of Fe(NO₃)₃·9H₂O on the MeOH solution of bpaeOH with NaN₃ for several days. Anal. calcd for C₃₀H₄₂Fe₂N₃₀O₆: C, 31.55; H, 3.71; N, 36.79. Found: C, 31.77; H, 3.59; N, 37.00. FT–IR (KBr, cm⁻¹): $\nu(\text{N}_3^-)$ 2077, 2061, 2028; $\nu(\text{C–H})$ 3082, 2924; $\nu(\text{C–O})$ 1048, 1026; $\nu(\text{C–N})$ 1606, 1346, 1320, 1290; $\nu(\text{C–C})$ 1435, 1384.

[Co(bpaeOH)(NCS)₂] (5). To an MeOH solution (5 mL) of Co(NO₃)₂·6H₂O (60 mg, 0.21 mmol) was added an MeOH solution (5 mL) of bpaeOH (50 mg, 0.21 mmol) and an MeOH solution (4 mL) of sodium thiocyanate (33 mg, 0.41 mmol). The mixture was stirred for 1 h at room temperature, and subsequently heated to reflux for 30 min. After cooling to room temperature, the resulting mixture was allowed to stand for 2 days. Purple crystals were formed and collected by filtration and washed with methanol and diethyl ether and dried in air (yield: 31 mg, 35%). Anal. calcd for C₁₆H₁₇CoN₃OS₂: C, 45.93; H, 4.10; N, 16.74; S, 15.33. Found: C, 45.70; H, 4.09; N, 17.00; S, 14.67. FT–IR (KBr, cm⁻¹): $\nu(\text{OH})$ 3436, 3230; $\nu(\text{SCN}^-)$ 2087, 2071; $\nu(\text{C–H})$ 2905; $\nu(\text{C–O})$ 1051, 1020; $\nu(\text{C–N})$ 1605, 1287; $\nu(\text{C–C})$ 1443.

[Co₃(bpaeO)₂(NO₃)(N₃)₄](NO₃) (6). To an MeOH solution (5 mL) of Co(NO₃)₂·6H₂O (120 mg, 0.41 mmol) was added an MeOH solution (5 mL) of bpaeOH (50 mg, 0.21 mmol) and an MeOH solution (7 mL) of sodium azide (54 mg, 0.82 mmol). The mixture was stirred for 1 h at room temperature. The color of the mixture became a dark red and then a dark red solid formed. The solid was collected by filtration and washed with methanol and diethyl ether and dried in air (yield: 115 mg, 63%). Dark red needle-shaped crystals of 6 suitable for X-ray crystal analysis were obtained by layering of the MeOH solution of Co(NO₃)₂·6H₂O on the MeOH solution of bpaeOH with NaN₃ for several days. Anal. calcd for C₂₈H₃₂Co₃O₈N₂₀: C, 35.25; H, 3.38; N, 29.39. Found: C, 35.14; H, 3.38; N, 29.53. FT–IR (KBr, cm⁻¹): $\nu(\text{N}_3^-)$ 2068, 2029; $\nu(\text{NO}_3^-)$ 1384, 1363; $\nu(\text{C–H})$ 3089, 3042, 2858; $\nu(\text{C–O})$ 1063, 1036; $\nu(\text{C–N})$ 1612, 1282; $\nu(\text{C–C})$ 1447.

X-Ray crystallographic data collection and refinement

Crystals of 1–6 were mounted on a CryoLoop[®] with Paratone[®] oil. Intensity data for all structures were collected with a Bruker APEX CCD-based diffractometer (Korea Basic Science Institute, Chonju Branch) and using Mo-K α radiation ($\lambda = 0.71073$ Å, graphite monochromator) at 173(2)–293(2) K. The raw data were processed to give structure factors using the Bruker SAINT program and corrected for Lorentz and polarization effects.¹³ The intensity data of 2–3 and 5–6 were corrected for absorption using the SADABS program with multi-scan data

($T_{\min}/T_{\max} = 0.861$ for **2**, 0.805 for **3**, 0.925 for **5**, and 0.756 for **6**).¹⁴ The crystal structures were solved by direct methods,¹⁵ and refined by full-matrix least-squares refinement using the SHELXL-97 computer program.¹⁶ The positions of all non-hydrogen atoms were refined with anisotropic displacement factors. All hydrogen atoms were placed using a riding model, and their positions were constrained relative to their parent atoms using the appropriate HFIX command in SHELXL-97, except the hydrogen of hydroxyl groups in **3** and **5**. Due to the disorder, one of two NO_3^- anions for **6** was treated with the SQUEEZE routine in the program PLATON¹⁷ and was omitted from the final refinements as atomic contributions, but are included in the computation of intensive properties. The crystallographic data and the result of refinements of **1–6** are summarized in Table 1.

Catalytic hydrocarbon oxidations upon treatment of **6** with *m*-chloroperoxybenzoic acid

To a mixture of substrate (0.1 mmol), cobalt complex **6** (0.001 mmol), and solvent (CH_3CN , 1 mL) was added *m*-chloroperoxybenzoic acid (MCPBA, 0.035 mmol). The mixture was stirred for 10 min at room temperature. Each reaction was monitored by GC–MS analysis with 20 μL aliquots being withdrawn periodically from the reaction mixture. All reactions were run at least in triplicate and the average product yields are presented. The product yields are based on MCPBA. In the competitive reaction of *cis*-2-hexene and *trans*-2-hexene, the amount of each substrate was 0.05 mmol.

Kinetic isotope effect study for the oxidation of benzyl alcohol by **6** and *m*-chloroperoxybenzoic acid

In order to improve the accuracy for measuring the amount of deuterated benzyl alcohol product, a 1 : 6 mixture of benzyl alcohol and deuterated benzyl alcohol was used. The reaction conditions were as follows: To a mixture of benzyl alcohol (0.02

mmol), deuterated benzyl alcohol (0.12 mmol), cobalt complex **6** (0.001 mmol), and solvent (CH_3CN , 1 mL) was added *m*-chloroperoxybenzoic acid (MCPBA, 0.035 mmol). The mixture was stirred for 10 min at room temperature. The reaction was monitored by GC–MS analysis of 20 μL aliquots withdrawn periodically from the reaction mixture. All reactions were run at least in triplicate and the average KIE values are presented.

Competitive reactions of styrene and *para*-substituted styrenes for Hammett plot

To a mixture of styrene (0.02 mmol) and *para*(X)-substituted styrene (0.02 mmol, X = $-\text{OCH}_3$, $-\text{CH}_3$, $-\text{Cl}$, $-\text{F}$, and $-\text{CN}$), cobalt complex **6** (0.001 mmol), and solvent (CH_3CN , 1 mL) was added *m*-chloroperoxybenzoic acid (MCPBA, 0.035 mmol). The mixture was stirred for 10 min at room temperature. The amounts of styrenes before and after reactions were determined by GC. The relative reactivities were determined using the following equation: $k_x/k_y = \log(X_f/X_i)/\log(Y_f/Y_i)$ where X_i and X_f are the initial and final concentrations of substituted styrenes and Y_i and Y_f are the initial and final concentrations of styrene.¹⁸

Results and discussion

Synthesis and characterization

The reaction of one equivalent of bpaeOH and 2 equiv of NaSCN with $\text{M}(\text{NO}_3)_2 \cdot x\text{H}_2\text{O}$ or $\text{Fe}(\text{BF}_4)_2 \cdot 6\text{H}_2\text{O}$ (M = Mn ($x = 4$), Co ($x = 6$)) in MeOH solution at room temperature affords the mononuclear complexes, $[\text{M}^{\text{II}}(\text{bpaeOH})(\text{NCS})_2]$ (**1**, pale yellow), $[\text{Fe}^{\text{II}}(\text{bpaeOH})(\text{NCS})_2]$ (**3**, orange–yellow), and $[\text{Co}^{\text{II}}(\text{bpaeOH})(\text{NCS})_2]$ (**5**, purple), in good yield, respectively. In the infrared (IR) spectra of **1**, **3**, and **5**, broad bands in the range of 3253–3423, 3248–3426, and 3230–3436 cm^{-1} , respectively, are displayed in which these correspond to O–H peaks. The strong peaks in the 2056–2068 (**1**), 2059–2077 (**3**), and 2071–2087 cm^{-1} (**5**)

Table 1 Summary of the crystallographic data for **1–6**

	1	2	3	4^c	5	6
Formula	$\text{C}_{16}\text{H}_{17}\text{MnN}_5\text{O}_5\text{S}_2$	$\text{C}_{14}\text{H}_{16}\text{MnN}_9\text{O}$	$\text{C}_{16}\text{H}_{17}\text{FeN}_5\text{O}_5\text{S}_2$	$\text{C}_{30}\text{H}_{38}\text{Fe}_4\text{N}_{30}\text{O}_4$	$\text{C}_{16}\text{H}_{17}\text{CoN}_5\text{O}_5\text{S}_2$	$\text{C}_{28}\text{H}_{32}\text{Co}_3\text{N}_{20}\text{O}_8$
M_r	414.41	381.30	415.32	1106.30	418.40	953.52
Crystal system	Monoclinic	Monoclinic	Monoclinic	Orthorhombic	Monoclinic	Monoclinic
Space group	$P2_1$	$P2_1/c$	$P2_1/n$	$Pbca$	$P2_1/n$	$P2/n$
$a/\text{\AA}$	8.3632(12)	8.6742(8)	8.4629(9)	13.780(4)	8.4373(7)	8.544(3)
$b/\text{\AA}$	11.6074(17)	13.3698(13)	11.5128(12)	13.921(4)	11.4202(9)	18.177(7)
$c/\text{\AA}$	9.7721(14)	13.6701(12)	19.611(2)	22.471(7)	19.3899(16)	12.538(5)
$\beta/^\circ$	93.997(3)	98.150(2)	94.807(3)		94.095(2)	101.358(8)
$V/\text{\AA}^3$	946.3(2)	1569.3(3)	1904.0(3)	4311(2)	1863.6(3)	1908.9(13)
Z	2	4	4	4	4	2
$D_c/\text{g cm}^{-3}$	1.454	1.614	1.449	1.705	1.491	1.659
T/K	173(2)	293(2)	195(2)	173(2)	200(2)	173(2)
$\lambda/\text{\AA}$	0.71073	0.71073	0.71073	0.71073	0.71073	0.71073
μ/mm^{-1}	0.932	0.867	1.025	1.396	1.159	1.365
Reflections collected	5965	11303	13975	30470	13476	13681
Independent reflections	4078	3870	4719	5362	4616	4737
R_{int}	0.0594	0.0488	0.0813	0.1362	0.0690	0.0836
R_1^a (4σ data)	0.0696	0.0436	0.0691	0.0481	0.0615	0.0766
wR_2^b (4σ data)	0.1315	0.0888	0.1521	0.0950	0.1303	0.1787
Flack parameter	0.05(3)	none	none	none	none	none
CCDC no.	806668	806667	806666	749014	806665	806664

^a $R_1 = \sum |F_o| - |F_c| / \sum |F_o|$. ^b $wR_2 = [\sum w(F_o^2 - F_c^2)^2 / \sum w(F_o^2)^2]^{1/2}$. ^c ref. 3

are assigned to coordinated thiocyanate ions.¹⁹ These complexes all have divalent metal ions such as Mn^{II}, Co^{II}, and Fe^{II}, indicative of weak coordination ability of the thiocyanate ion (*vide infra*). Dark gray crystals of [Mn^{III}(bpaeO)(N₃)₂] (**2**) were obtained in 45% yield from a solution of bpaeOH, Mn(NO₃)₂·4H₂O (1 : 1) and NaN₃ (2 eq) in methanol at room temperature in the presence of air. The sharp and strong peaks at 2044–2066 cm⁻¹ for **2** are assigned to coordinated azide ions.¹⁹ Interestingly, the hydroxyl group of bpaeOH ligand is deprotonated and the manganese ion is oxidized to 3+ as the azide ions are coordinated to the manganese ion. That is, two manganese complexes **1** and **2** are formed in different oxidation states, *e.g.* 2+ and 3+, depending on the coordinated anions. From a solution of bpaeOH, Fe(NO₃)₃·9H₂O, and NaN₃ (1 : 2 : 6) in methanol at ambient temperature in the presence of air, a reddish-brown precipitate of **4** was obtained in 77% yield. Compound **4** in the IR spectra shows strong bands at 2077, 2061, and 2028 cm⁻¹ which is where the ν_{as} bands for coordinated azide ions appear.¹⁹ Contrary to **3**, very interestingly, a zigzag tetranuclear Fe(III) complex **4** is obtained. From a solution of bpaeOH, Co(NO₃)₂·6H₂O, and NaN₃ (1 : 2 : 4) in methanol at ambient temperature in the presence of air a dark red precipitate of [Co₃(bpaeO)₂(NO₃)(N₃)₄](NO₃) (**6**) was obtained in 63% yield. Compound **6** in the IR spectra shows very sharp and strong peaks at 2029–2068 cm⁻¹ which are assigned to coordinated azide ions.¹⁹ Strong bands observed at 1364–1384 cm⁻¹ indicate the nitrate anions. Contrary to **5**, the cobalt(II) ions in **6** are oxidized partially by using the azide ion, which is a more oxidizing agent compared to the thiocyanate ion. As a result, mixed-valence trinuclear cobalt complex **6** is obtained. The composition and structure of all compounds were determined by elemental analysis, infrared spectrum, solid state magnetochemistry, and single crystal X-ray diffraction analysis.

Description of crystal structures

Structure of 1. Compound **1** crystallizes in the monoclinic *P*₂₁ space group, and the unit cell includes two mononuclear complexes, and the ORTEP drawing of **1** is shown in Fig. 1, and the selected bond lengths and angles are listed in Table 2.

Table 2 Selected bond distances (Å) and angles (°) for **1**, **2**, **3** and **5**

	1	2	3	5
M1–N1	2.267(5)	2.232(3)	2.182(5)	2.138(4)
M1–N2	2.300(4)	2.188(3)	2.214(4)	2.149(4)
M1–N3	2.269(5)	2.240(3)	2.180(5)	2.129(4)
M1–N4	2.099(5)	1.994(3)	2.124(6)	2.092(4)
M1–N5	2.184(5)		2.017(5)	2.013(4)
M1–O1	2.298(4)	1.856(2)	2.256(4)	2.205(3)
M1–N7		2.010(3)		
O1–M1–N1	90.92(16)	94.24(11)	85.79(17)	86.21(15)
O1–M1–N2	75.54(15)	83.19(11)	77.68(16)	80.44(14)
O1–M1–N3	83.63(17)	89.97(11)	86.25(17)	88.15(15)
O1–M1–N4	89.2(2)	175.37(13)	173.40(18)	89.88(16)
O1–M1–N5	168.69(17)		89.56(18)	174.40(17)
O1–M1–N7		90.09(12)		
N1–M1–N2	73.91(17)	75.55(11)	75.74(19)	78.52(16)
N1–M1–N3	148.76(18)	151.45(11)	151.74(19)	156.56(16)
N2–M1–N3	74.94(17)	76.95(11)	76.08(18)	78.11(15)
N4–M1–N5	99.4(2)		96.10(20)	94.69(18)
N4–M1–N7		93.98(14)		

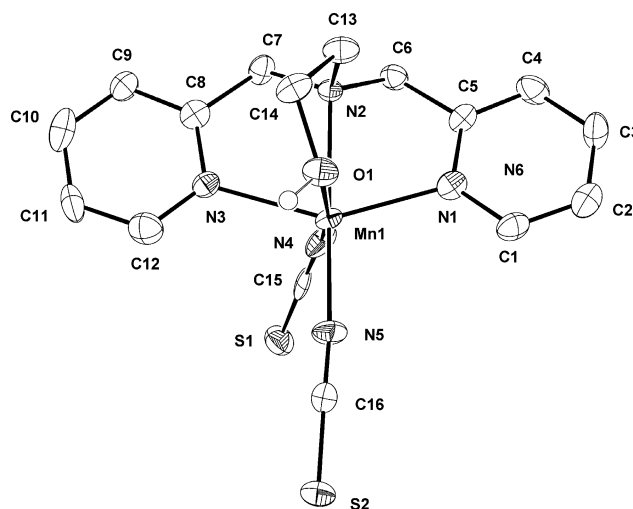


Fig. 1 Structure of the neutral complex [Mn^{II}(bpaeOH)(NCS)₂] in crystals of **1**. Those of the neutral complexes in crystals **3** (Fe) and **5** (Co) are similar and not shown. The atoms are represented by 50% probable thermal ellipsoids. The hydrogen atom on the hydroxyl group is shown as a small open circle; all other H-atoms are omitted for clarity.

The coordination geometry around the Mn(II) can be described as distorted octahedral, consisting of the three N atoms and one O atom from the bpaeOH ligand, and two N atoms of thiocyanate anions. The average Mn–L_{bpaeOH} bond length is 2.287(2) Å and the Mn–N_{thiocyanato} bond lengths are in the range of 2.099(5) to 2.184(5) Å. The Mn–N_{thiocyanato} bond lengths are comparable to those of [Mn^{II}(TPyA)(NCS)₂].CH₃CN (*i.e.* 2.110(4) and 2.171(4) Å) (TPyA = tris(2-pyridylmethyl)amine).²⁰ From the bond lengths, the spin state of the manganese(II) ion is believed to be high-spin (*d*⁵, *S* = 5/2).²¹ The bond angles relating to the manganese atom lie from 73.91(17) to 168.69(17)°. The thiocyanate ions are nearly linear and show bent coordination modes with the manganese atom (\angle N4C15S1; 179.0(6)°, \angle N5C16S2; 179.0(5)°, \angle Mn1N4C15; 172.3(5)°, \angle Mn1N5C16; 142.0(5)°). The hydroxyl group of **1** is involved in a hydrogen-bonding interaction with the sulfur atom of thiocyanate ion belonging to an adjacent manganese atom: O1...S2 (*x* + 1, *y*, *z*) 3.207(4) Å, \angle O1H1AS2 167.4°. Due to the interactions, compound **1** is linked to form a one-dimensional chain extending along the *a* axis as shown in Fig. 2. Additionally, the pyridyl groups of **1** are involved in extensive π – π stacking interactions with offset face-to-face π – π interactions.²² Between the monomers, the pyridine ring involving N1 undergoes the offset π – π interaction with the pyridine group involving N3 (*–x*, *y* – 0.5, *–z*), which is positioned at the neighboring monomer. The inter-planar separation of the pyridine rings is 3.63(1)–4.09(2)

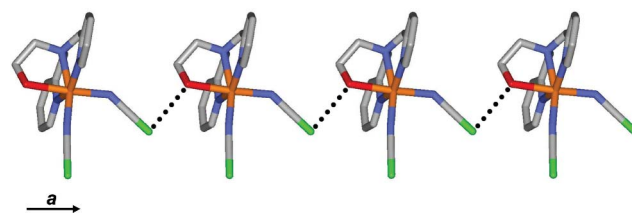


Fig. 2 A one-dimensional chain of **1** formed by hydrogen-bonding interactions between the hydroxyl group and the sulfur atom of thiocyanate ion. Hydrogen bonds are indicated by dotted lines.

Å (centroid...centroid, 4.08 Å) and the dihedral angle between the pyridine ring planes is 5.9(1)°. Due to the inter-monomer offset face-to-face π - π interactions, **1** forms a 2-D network.

Structure of 2. Compound **2** crystallizes in the monoclinic $P2_1/c$ space group, and the unit cell includes four mononuclear complexes, and the ORTEP drawing of **2** is shown in Fig. 3, and the selected bond lengths and angles are listed in Table 2. The manganese(III) ion is coordinated by three N atoms and one O atom from bpaeO⁻ ligand, and two N atoms of the azide anions. Thus, the coordination geometry of **2** can be regarded as being same as that of **1**. The average Mn-L_{bpaeO} bond length is 2.064(1) Å and the Mn-N_{azido} bond lengths are in the range of 1.994(3) to 2.010(3) Å. The Mn-N bond lengths are longer than 2.00 Å in accordance with a high-spin Mn^{III} complex ($S = 2$).²³ Bond valence sum (BVS) calculations give the valence sums of 2.09 for Mn(II) in **1** and 3.06 for Mn(III) in **2**.²⁴ The results indicate that the manganese ions in **1** and **2** are divalent and trivalent, respectively. The bond angles relating to the manganese(III) ion lie from 75.55(11) to 175.37(13)°. The azide ions are nearly linear and show bent coordination modes with the manganese atom ($\angle N4N5N6$; 176.9(4)°, $\angle N7N8N9$; 177.7(4)°, $\angle Mn1N4N5$; 125.7(3)°, $\angle Mn1N7N8$; 118.1(3)°). The pyridyl groups of **2** are involved in extensive π - π stacking interactions with offset face-to-face π - π interactions.²² Between the monomers, the pyridine ring involving N1 undergoes the offset π - π interaction with the pyridine group involving N3 ($x - 1, y, z$), which is positioned at the neighboring monomer. The inter-planar separation of the pyridine rings is 3.07(1)–3.36(1) Å (centroid...centroid, 3.70 Å) and the dihedral angle between the pyridine ring planes is 7.2(2)°. Due to the inter-monomer offset face-to-face π - π interactions, **2** forms a 1-D chain structure along the a axis (Fig. 4).

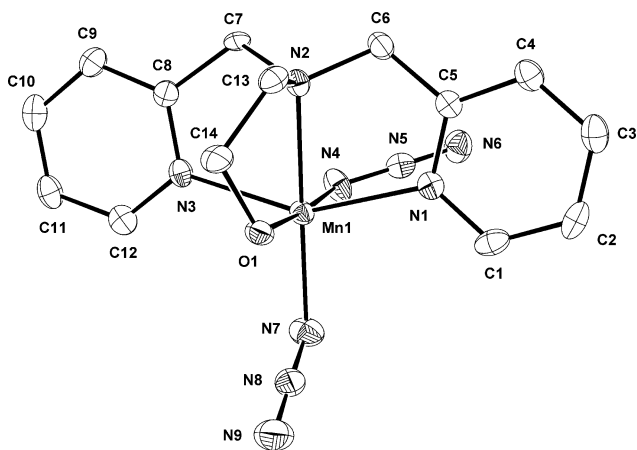


Fig. 3 Structure of the neutral complex $[Mn^{III}(bpaeO)(N_3)_2]$ in crystals of **2**. The atoms are represented by 50% probable thermal ellipsoids. All hydrogen atoms are omitted for clarity.

Structure of 3. The structure of compound **3** is similar to that of **1**. Compound **3** crystallizes in the monoclinic $P2_1/n$ space group, and the unit cell includes four mononuclear complexes, and the ORTEP drawing of **3** is shown in Fig. 1, and the selected bond lengths and angles are listed in Table 2. The coordination geometry around the iron(II) ion can be described as a distorted octahedron, consisting of the three N atoms

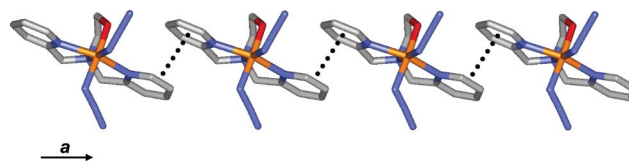


Fig. 4 A one-dimensional chain of **2** formed by offset face-to-face π - π interactions between the pyridine rings of the bpaeO⁻ ligand. The interactions are indicated by dotted lines.

and one O atom from the bpaeOH ligand, and two N atoms from thiocyanate anions. The average Fe-L_{bpaeOH} bond length is 2.214(2) Å and the Fe-N_{thiocyanato} bond lengths are in the range of 2.017(5) to 2.124(6) Å. Both the average Fe-N_{pyridine} distance (2.181(4) Å) and the Fe-N_{amine} distance (2.214(4) Å) in **3** are comparable to those found in the N4-coordinate high-spin iron(II) complex, $[(LBz)_2Fe^{II}Cl_2] \cdot H_2O$ ($LBz_2 = N,N'$ -bisbenzyl- N,N' -bis(2-pyridylmethyl)ethane-1,2-diamine).²⁵ The bond angles relating to the iron atom lie from 75.74(19) to 173.40(18)°. The thiocyanate ions are nearly linear and show a bent coordination mode with the iron(II) ion ($\angle N4C15S1$; 179.3(6)°, $\angle N5C16S2$; 179.2(6)°, $\angle Fe1N4C15$; 152.1(5)°, $\angle Fe1N5C16$ 169.1(5)°). The hydroxyl group of **3** is involved in a hydrogen-bonding interaction with the sulfur atom of the thiocyanate ion belonging to an adjacent iron(II) ion: O1...S1 ($x - 1, y, z$) 3.190(5) Å, $\angle O1H1AS1$ 156(7)°. Due to the interactions, compound **3** is linked to form a one-dimensional chain extending along a axis as shown in Fig. 5. Furthermore, between the 1-D chains, the sulfur atom of coordinated thiocyanate ion undergoes a sulfur-sulfur interaction, which leads to a ladder-like chain extending along the a axis (Fig. 5). The distance between the sulfur atoms is 3.441(3) Å, which is shorter than the van der Waals radii (3.60 Å).²⁶

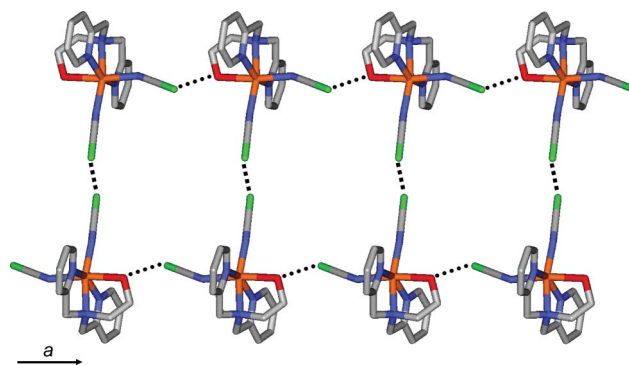


Fig. 5 Perspective view of **3** showing the ladder-like 1-D chains. That of **5** is similar and not shown. The hydrogen bonding interactions and the sulfur-sulfur interactions are indicated as \cdots and \blacksquare , respectively.

Structure of 4. Compound **4** crystallizes in the orthorhombic $Pbca$ space group, and the unit cell includes four tetranuclear complex molecules, and the ORTEP drawing of **4** is shown in Fig. 6.³ Table 3 exhibits selected bond distances (Å) and angles (°) for **4**. The asymmetric unit of **4** contains two different iron(III) ions, one (Fe1) is coordinated with a deprotonated bpaeO⁻ ligand, an azide ion, and a methoxy group, and the other (Fe2) is bonded to four azide ions and two oxygens from the bpaeO⁻ ligand and a methoxy group. That is, a $Fe_2(bpaeO)(CH_3O)(N_3)_4$ unit results from the bridging of two iron(III) ions through one μ_2 -O bridging CH_3O^-

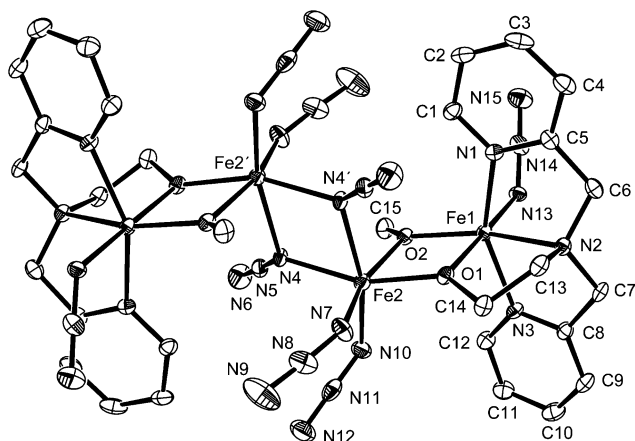


Fig. 6 Molecular structure of **4** with thermal ellipsoids at 30% probability.³ All hydrogen atoms are omitted for clarity. Symmetry code: (') $1 - x, -y, 1 - z$.

Table 3 Selected bond distances (Å) and angles (°) for **4**

Fe1–O1	2.001(3)	Fe2–O1	1.979(3)
Fe1–O2	1.936(3)	Fe2–O2	2.087(3)
Fe1–N1	2.141(3)	Fe2–N4	2.100(3)
Fe1–N2	2.215(3)	Fe2–N7	1.997(4)
Fe1–N3	2.115(3)	Fe2–N10	2.018(4)
Fe1–N13	2.005(4)	Fe2–N4 ⁱ	2.155(3)
N1–Fe1–O1	94.67(12)	O1–Fe2–O2	73.13(11)
N1–Fe1–O2	106.19(13)	O1–Fe2–N4	159.59(13)
N1–Fe1–N2	75.06(13)	O1–Fe2–N4 ⁱ	90.28(12)
N1–Fe1–N3	152.25(14)	O1–Fe2–N7	89.91(14)
N1–Fe1–N13	87.17(14)	O1–Fe2–N10	104.94(15)
N2–Fe1–O1	80.70(12)	O2–Fe2–N4	94.52(13)
Fe1–O1–Fe2	106.27(12)	Fe1–O2–Fe2	104.60(12)
Fe2–N4–Fe2 ⁱ	106.78(15)		

Symmetry transformations used to generate equivalent atoms: (i) $-x + 1, -y, -z + 1$.

ligand and the terminal O_{alkoxo} of the tetradentate bpaehO^- ligand. The two $\text{Fe}_2(\text{bpaehO})(\text{CH}_3\text{O})(\text{N}_3)_4$ units are related by symmetry through an inversion center situated at the barycenter of the complex. That is, this new type of a zigzag tetranuclear iron(III) structure results from the bridging of two $\text{Fe}_2(\text{bpaehO})(\text{CH}_3\text{O})(\text{N}_3)_4$ dinuclear moieties through two μ_2 -*N*-azido anions. The amine nitrogen and the bridged ethoxyl oxygen atoms lie in the plane of the Fe_2O_2 core. The pyridine nitrogen atoms occupy two axial positions in the octahedron. The distorted octahedral coordination sphere of the internal iron (Fe2) ion involves a N_4O_2 donor set including: two $\text{N}(\text{N}_3^-)$, two μ_2 - $\text{N}(\text{N}_3^-)$, μ_2 - $O_{\text{alkoxo}}(\text{bpaehO}^-)$, and μ_2 - $O_{\text{alkoxo}}(\text{CH}_3\text{O}^-)$. The coordination environment of the external iron (Fe1) ion shows a N_4O_2 donor set including two $\text{N}_{\text{py}}(\text{bpaehO}^-)$, $\text{N}_{\text{amine}}(\text{bpaehO}^-)$, $\text{N}(\text{N}_3^-)$, μ_2 - $O_{\text{alkoxo}}(\text{bpaehO}^-)$, and μ_2 - $O_{\text{alkoxo}}(\text{CH}_3\text{O}^-)$. Complex **4** has the average Fe1–N, Fe1–O, Fe2–N, and Fe2–O bond distances of 2.133(2), 1.969(2), 2.084(2), and 2.033(2) Å, respectively. Interestingly, the average Fe1–N/O and Fe2–N/O bond lengths are very similar to each other (2.051(1) Å for Fe1 and 2.059(1) Å for Fe2), and indicate that the oxidation states and electronic structures of the iron ions are 3+ and high spin, respectively. Additionally, by analysis of BVS calculations for **4** (2.95 (Fe1) and 3.03 (Fe2)), both iron ions correspond to the 3+ valence states.²⁴ In **4**, the oxidation states of iron ions

were identified as 3+, as demonstrated by the powder zero-field Mössbauer spectrum (isomer shifts of 0.21 and 0.28 mm s^{-1} and quadrupole-splitting parameters of 0.85 and 0.38 mm s^{-1} for six-coordination of Fe1 and Fe2).³ Furthermore, the average N–N bond distance of the azide ions is 1.177(2) Å, indicative of the delocalization of the azide ions. The intradinuclear Fe1...Fe2 and interdinuclear Fe2...Fe2' ($1 - x, -y, 1 - z$) distances between adjacent iron centers are 3.185(1) and 3.416(2) Å, respectively.

Structure of 5. Compound **5** crystallizes in the monoclinic $P2_1/n$ space group, and the unit cell includes four mononuclear complexes, and the ORTEP drawing of **5** is shown in Fig. 1, and the selected bond lengths and angles are listed in Table 2. The coordination geometry around the cobalt(II) ion can be described as a distorted octahedron. Three nitrogen atoms and an oxygen atom of the bpaehO ligand constitute an N_3O donor set around the cobalt(II) ion and the remaining coordination positions are occupied by the thiocyanate anions. The coordination configuration of bpaehO around the cobalt(II) ion apparently differs from that of the analogous N_4 -ligand, LBZl_2 .²⁵ The $\text{Co}-L_{\text{bpaehO}}$ bond length is 2.131(2) Å and the $\text{Co}-\text{N}_{\text{thiocyanato}}$ bond lengths are in the range of 2.013(4) to 2.092(4) Å. The bond angles relating to the cobalt(II) ion lie from 78.11(15) to 174.40(17)°. The thiocyanate ions are nearly linear and show a bent coordination mode with the cobalt(II) ion ($\angle\text{N4C15S1}$; 179.6(5)°, $\angle\text{N5C16S2}$; 179.3(5)°, $\angle\text{Co1N4C15}$; 151.3(4)°, $\angle\text{Co1N5C16}$; 170.5(4)°). The hydroxyl group of **5** is involved in a hydrogen-bonding interaction with the sulfur atom of the thiocyanate ion belonging to an adjacent cobalt(II) ion: $\text{O1} \cdots \text{S1}$ ($x - 1, y, z$) 3.196(4) Å, $\angle\text{O1H1S1}$ 162(6)°. Due to the interactions, compound **5** is linked to form a one-dimensional chain extending along the *a* axis as shown in Fig. 5. Furthermore, between the 1-D chains, the sulfur atom of coordinated thiocyanate ion undergoes a sulfur–sulfur interaction, which gives rise to a ladder-like chain extending along the *a* axis (Fig. 5). The distance between the sulfur atoms is 3.417(3) Å, which is shorter than the van der Waals radii (3.60 Å).²⁶ The structure of **5** is isomorphous to those of **1** and **3**. Furthermore, the BVS calculations give the valence sums of 2.07 for Fe(II) in **3** and 2.11 for Co(II) in **5**.²⁴ The values indicate that the iron and cobalt ions in **3** and **5**, respectively, are divalent.

Structure of 6. Compound **6** crystallizes in the monoclinic $P2_1/n$ space group, and the unit cell includes two trinuclear complexes and two nitrate counteranions, and the ORTEP drawing of **6** is shown in Fig. 7. The selected bond lengths and angles are listed in Table 4. The core structure of **6** is composed of one mixed-valence $\text{Co}^{\text{III}}\text{Co}^{\text{II}}\text{Co}^{\text{III}}$ trimer and one nitrate anion. The central cobalt(II) ion is bonded to four oxygen atoms, $\text{Co}-\text{O}(\text{av.}) = 1.999(3)$ Å and to two bridged nitrogen atoms, $\text{Co}-\text{N}(\text{av.}) = 2.211(4)$ Å. The terminal cobalt(III) ions on the other hand are bonded to five nitrogens, $\text{Co}-\text{N}(\text{av.}) = 1.946(2)$ Å and to one bridged methoxy group, $\text{Co}-\text{O} = 1.889(4)$ Å. The latter distances compare well with those previously reported for cobalt(III) ions,⁸ while the former are much longer and suggest a cobalt(II) ion. In fact the difference in the average $\text{Co}-\text{N}/\text{O}$ distance of the central and external cobalt ions (~ 0.15 Å) corresponds well to the difference in octahedral ionic radii of cobalt(II) and cobalt(III) ions.²⁶ In **6** the cation is formulated as $[(\text{bpaehO})(\text{N}_3)\text{Co}^{\text{III}}(\mu-1,1-\text{N}_3)\text{Co}^{\text{II}}(\eta^2-\text{NO}_3^-)(\mu-1,1-\text{N}_3)\text{Co}^{\text{III}}(\text{N}_3)(\text{bpaehO})]^+$. Two bpaehO s are deprotonated by coordination to the cobalt ion. This result is in line with the observed

Table 4 Selected bond distances (Å) and angles (°) for **6**

Co1–O1	1.889(4)	Co1–N7	1.942(5)
Co1–N1	1.948(5)	Co2–O1	1.965(4)
Co1–N2	1.955(6)	Co2–O2	2.136(8)
Co1–N3	1.932(6)	Co2–N4	2.211(5)
Co1–N4	1.954(6)		
O1–Co1–N1	92.5(2)	N2–Co1–N3	83.5(3)
O1–Co1–N2	87.0(2)	N2–Co1–N7	93.4(2)
O1–Co1–N3	90.5(2)	N3–Co1–N7	90.1(2)
O1–Co1–N7	179.3(2)	N4–Co1–N7	97.7(2)
N1–Co1–N2	85.1(2)	O1–Co2–O1 ⁱⁱ	122.6(3)
N1–Co1–N3	168.1(2)	O2–Co2–O2 ⁱⁱ	58.5(5)
N1–Co1–N7	86.9(2)	N4–Co2–N4 ⁱⁱ	156.5(3)

Symmetry transformations used to generate equivalent atoms: (ii) $-x + 3/2, y, -z + 3/2$.

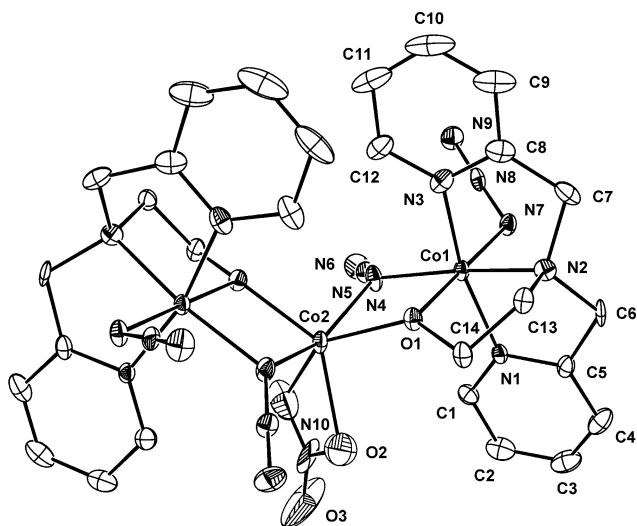


Fig. 7 Molecular structure of **6** with thermal ellipsoids at 30% probability. All hydrogen atoms and non-coordinated nitrate anion are omitted for clarity.

distance between oxygen and the terminal cobalt ion, which is slightly shorter than that observed in **5**. The distorted octahedral coordination sphere of the central cobalt (Co2) involves an N_2O_4 donor set including: two μ_2 -N(N_3^-), two μ_2 -O_{alkoxo}(bpaeO⁻), and two O(η^2 -NO₃⁻). The octahedral coordination sphere of the external cobalt (Co1) shows an N_5O donor set including two N_{py} (bpaeO⁻), N_{amine} (bpaeO⁻), N(N_3^-), μ_2 -N(N_3^-), and μ_2 -O_{alkoxo}(bpaeO⁻). In particular, the distortion from ideal octahedral geometry of the central cobalt(II) ion is due to the coordination bond of the nitrate ion (η^2 -NO₃⁻), which forms a four-membered ring with cobalt ion ($\angle O_2Co_2O_2(-x + 1.5, y, -z + 1.5) = 58.5(5)^\circ$). The average N–N bond distance of azide ions is 1.188(4) Å and the bonds are delocalized. The Co^{III}–Co^{II} distance within the trimeric cation is 3.105(1) Å, lower than those (3.7121(16) and 3.828(9) Å) found in the cases of Co^{II}–Co^{II} systems.²⁷ The BVS calculation for Co1 (3.46) agreed with the 3+ valence state, whereas that for Co2 (2.12) indicated the 2+ valence state in **6**.²⁴ That is, this strongly demonstrates the +2 oxidation state for central cobalt ion and the +3 oxidation states for terminal cobalt ions.

Magnetic properties. Variable-temperature 2 or 5 to 300 K magnetic susceptibility, χ , measurements on polycrystalline sam-

ples of **1–6** were investigated. Complex **1** has a room-temperature effective moment, $\mu_{\text{eff}} [= (8 \chi T)^{1/2}]$, of 5.88 μ_B , indicative of a high spin ($S = 5/2$) configuration. This value is slightly lower than the expected spin-only value of 5.92 μ_B . On lowering the temperature, the μ_{eff} values are almost constant and maintain the high-spin state (5.70 μ_B at 3 K) (Fig. 8). The best fit has $g = 1.985$, $|D| = 0.01 \text{ cm}^{-1}$, and $\theta = -0.14 \text{ K}$, which is an $S = 5/2$ ground state.^{12,28} This result is consistent with those displayed by several high-spin manganese(II) complexes such as [Mn^{II}(en)₃]Br₂ and [Mn^{II}([9]aneN₂S)₂](ClO₄)₂ (en = ethylenediamine, [9]aneN₂S = 1-thia-4,7-diazacyclononane).²⁹ The value of zero-field splitting (zfs) parameter ($|D|$) in **1** is in good agreement with [Mn^{II}([9]aneN₃)₂](ClO₄)₂ ($|D| = 0.09 \text{ cm}^{-1}$, [9]aneN₃ = 1,4,7-triazacyclononane) and all known Mn^{II} protein species ($|D| < 0.5 \text{ cm}^{-1}$).^{29,30} In complex **2**, the effective moment, $\mu_{\text{eff}} [= (8 \chi T)^{1/2}]$, at 300 K is 4.91 μ_B . This value is a little higher than the expected spin-only value of 4.89 μ_B , indicative of a high spin Mn^{III} ($S = 2$) configuration. On lowering the temperature, the μ_{eff} values are nearly constant and maintain the high-spin state (4.74 μ_B at 5 K). The best fit has $g = 2.014$, and $|D| = 1.999 \text{ cm}^{-1}$ (Fig. 8).¹² The zero-field splitting (zfs) parameter of **2** is very similar those found for Mn^{III} high-spin complexes.³¹

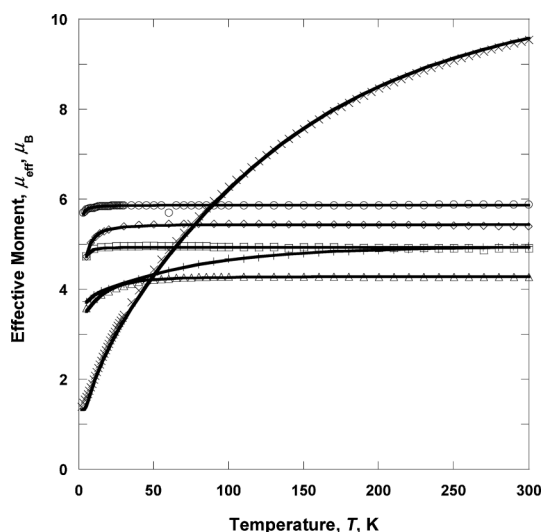


Fig. 8 Temperature dependence of the effective magnetic moment, $\mu_{\text{eff}}(T)$, of complexes **1–6** [**1** (○), **2** (□), **3** (◇), **4** (×), **5** (+), **6** (△)]. Solid lines represent best fits by using parameters given in the text.

Compound **3** has a 300 K effective magnetic moment of 5.40 μ_B that decreases monotonically with decreasing temperature to 4.72 μ_B at 5 K. This is higher than 4.89 μ_B , expected for $g = 2$ $S = 2$ Fe^{II} ion. On lowering the temperature, the μ_{eff} values are almost constant and decrease rapidly on further cooling below 50 K, indicative of zero-field splitting and/or intermolecular interactions. The best fit from magnetic susceptibility has $g = 2.219$ and $|D| = 6.45 \text{ cm}^{-1}$ (Fig. 8).¹² The zero-field splitting (zfs) parameter has a typically large value as a non-Kramers (integer spin) ion and is in good agreement with high-spin Fe^{II} zero-field splitting parameters (5–20 cm^{-1}).³² As reported earlier,³ complex **4** has a room-temperature moment of 9.54 μ_B/Fe_4 , in accord with the moments of tetranuclear complexes containing high-spin Fe^{III} ions. $\mu_{\text{eff}}(T)$ decreases monotonically with decreasing temperature to 1.39 μ_B/Fe_4 at 2 K. It should be noted that the continuous

decrease in $\mu_{\text{eff}}(T)$ with decreasing temperature from 300 to 2 K is suggestive of an antiferromagnetic interaction in **4**. However, as modelled, this could be only due to a stronger antiferromagnetic coupling than the ferromagnetic one in a system having both ferromagnetic and antiferromagnetic interactions. A satisfactory fit of data has been obtained using the spin-Hamiltonian operator for a zigzag tetranuclear system of four high-spin iron(III) with spin $S_a = S_b = S_c = S_d = 5/2$ ($H = -2J_1(S_a \cdot S_b + S_c \cdot S_d) - 2J_2(S_b \cdot S_c)$).¹² The best fit had $J_1 = -14.3 \text{ cm}^{-1}$, $J_2 = 9.8 \text{ cm}^{-1}$, $g = 2.00$, and the spin impurity, $\rho = 0.05$ (Fig. 8). The coupling constant (J_1) through the bridging oxygen atoms is expected to be antiferromagnetic and is consistent with value for $[\text{Fe}_2(\text{salam})(\text{OH})_2] \cdot 2\text{H}_2\text{O} \cdot 2\text{py}$ (salam = *N,N'*-ethylenebis(salicylamine), $J = -10.4 \text{ cm}^{-1}$).³³ Contrary to J_1 , the ferromagnetic coupling constant (J_2) via the end-on bridging mode in **4** is almost twice that reported for the $[\text{Fe}_2(\text{N}_3)_{10}]^{4-}$ anion ($J = 4.8 \text{ cm}^{-1}$), even though the angles of Fe–N–Fe are similar (106.0 and 106.8°).³⁴ Interestingly, **4** exists clearly both ferromagnetic and antiferromagnetic couplings within the tetranuclear unit, which is different to reported linear tetranuclear iron(II) compounds.³⁵

As shown in Fig. 8, the effective moment, $\mu_{\text{eff}} [= (8 \chi T)^{1/2}]$, value of **5** at 300 K is $4.94 \mu_{\text{B}}$, suggesting that the cobalt(II) ion is in the high-spin state. This value is larger than the spin-only value ($3.87 \mu_{\text{B}}$) for a high-spin Co^{II} , indicative of the strong spin-orbit coupling. On lowering the temperature, $\mu_{\text{eff}}(T)$ decreases gradually with decreasing temperature to $3.72 \mu_{\text{B}}/\text{Co}$ at 5 K. The decrease of the magnetic moment at low-temperature (<150 K) is most likely due to the strong spin-orbit coupling of Co^{II} . The spin-orbit coupling contributes to the zero-field splitting. The best fit from the data has $g = 2.580$, $|D| = 87.9 \text{ cm}^{-1}$ and $\theta = -0.575 \text{ K}$ (TIP = $100 \times 10^{-6} \text{ emu mol}^{-1}$). As shown in Fig. 8, the fit of the observed $\mu_{\text{eff}}(T)$ for **5** displays a very large *D*-value. The zero-field splitting parameter between the $\pm 1/2$ and $\pm 3/2$ Kramers doublets is comparable to that for $[\text{Co}(\text{Me}_6\text{tren})\text{Cl}]\text{Cl}$ ($|D| = 52.8 \text{ cm}^{-1}$, $\text{Me}_6\text{tren} = \text{tris}[2\text{-(dimethylamino)ethyl}]\text{amine}$).³⁶ The trinuclear compound **6** is composed of two low-spin Co^{III} as wingtip ions and one high-spin Co^{II} as the central ion, *i.e.* $\text{Co}^{\text{III}}(S = 0) - \text{Co}^{\text{II}}(S = 3/2) - \text{Co}^{\text{III}}(S = 0)$. The wingtip cobalt(III) ions are diamagnetic, while the central cobalt(II) ion is paramagnetic ($S = 3/2$). The effective magnetic moment at 300 K of the trinuclear complex **6** is measured to be $4.27 \mu_{\text{B}}$ ($3.58 \mu_{\text{B}}$ at 5 K), which is larger than that of the spin-only value ($3.87 \mu_{\text{B}}$) for a high-spin Co^{II} and corresponds to the strong spin-orbit coupling. The decrease of the magnetic moment at low-temperature (<40 K) is most likely due to the strong spin-orbit coupling of Co^{II} . The best fit of the magnetic data has $g = 2.212$ and $|D| = 18.2 \text{ cm}^{-1}$ (Fig. 8). The zero-field splitting parameter is comparable to those for $[\text{Co}(\text{salophen})(2\text{-methylimidazole})]$ ($|D| = 22.6 \text{ cm}^{-1}$) and $\text{CoCl}_2(\text{PPh}_3)_2$ ($|D| = 14.8 \text{ cm}^{-1}$) (salophen = *N,N'*-phenylenebis(salicylaldiminato) dianion, Ph = phenyl).³⁷

Hydrocarbon oxidations with the cobalt complex **6**

Since manganese, iron and cobalt have continuously gained prominence as catalysts for numerous transformations such as olefin epoxidation, alcohol oxidation, and *etc.*,³⁸ the reactivity of the complexes **1–6** as catalysts was examined in the epoxidation reaction and alcohol oxidation of a wide range of olefin and alcohol substrates with various oxidants such as H_2O_2 , *tert*-butyl

hydroperoxide and *m*-chloroperoxybenzoic acid (MCPBA). Only the combination of cobalt complex **6** and MCPBA was effective for the olefin epoxidation and alcohol oxidation and CH_3CN was the best solvent found for the oxidation reactions. To a mixture of substrate (0.1 mmol), cobalt complex **6** (0.001 mmol), and solvent (1 mL; CH_3CN) was added MCPBA (0.035 mmol). This mixture was stirred for 10 min at room temperature. We confirmed that direct substrate oxidation by MCPBA was negligible (occurring over a period of 10–60 min) whereas oxygen transfer reactions catalyzed by the cobalt complex **6** occur in less than one minute after the addition of the peroxybenzoic acid. Addition of a further portion of MCPBA regenerated the catalytic cycle with the same yield as the first cycle, indicating that the catalyst is robust under the conditions used.

Under the optimized conditions, reactions with olefins in the presence of **6** resulted predominantly in the formation of epoxides as shown in Table 5. Cyclic olefins such as cyclopentene, cycloheptene, and cyclooctene were oxidized to the corresponding epoxides in good yields (60–90%; entries 1–3). The terminal olefin 1-hexene, which is notoriously resistant to oxidation, was also oxidized to 1-hexene oxide with moderate yield (48.5%, entry 4) under these conditions. The reaction of cyclohexene produced mainly the epoxidation product (65.0%), along with cyclohexen-1-one (yield 4.8%) and cyclohexenol (yield 5.8%) as the minor allylic hydrogen abstraction products (entry 5), indicating that free radical oxidation reactions were almost not involved in the olefin epoxidation reactions.³⁹ *cis*-2-Hexene was used to probe the stereochemistry of the reaction, with *cis*-2-hexene oxide being produced as the major species (74.5%) along with some amounts of *trans*-2-hexene oxide (17.0%) (entry 6). This result indicates that the catalytic epoxidation reaction occurs with approximately 63% stereochemical retention. *trans*-2-Hexene was oxidized exclusively to *trans*-2-hexene oxide (entry 7). In the competitive epoxidation of *cis*- and *trans*-2-octene, the ratio of *cis*- to *trans*-2-octene oxide

Table 5 Hydrocarbon oxidations by MCPBA with cobalt catalyst **6** in CH_3CN at room temperature^a

Entry	Substrate	Product	Yield (%) ^b	TN ^c
1	Cyclopentene	Epoxide	59.5 ± 1.4	21.0
2	Cycloheptene	Epoxide	90.4 ± 3.3	31.5
3	Cyclooctene	Epoxide	78.1 ± 3.7	27.3
4	1-Hexene	Epoxide	48.5 ± 0.5	17.2
5	Cyclohexene	Epoxide	65.0 ± 1.7	22.8
		2-Cyclohexene-1-ol	5.8 ± 0.4	2.1
		2-Cyclohexenone	4.8 ± 0.6	1.7
6	<i>cis</i> -2-Hexene	<i>cis</i> -Oxide	74.5 ± 2.1	26.3
		<i>trans</i> -Oxide	17.0 ± 0.6	6.0
7	<i>trans</i> -2-Hexene	<i>trans</i> -Oxide	84.2 ± 1.2	29.4
8	<i>cis</i> -/ <i>trans</i> -2-Octene	<i>cis</i> -/ <i>trans</i> -Oxide	1.7	—
9	styrene	Epoxide	64.3 ± 0.3	22.4
		Benzaldehyde	11.6 ± 0.1	3.9
		Phenylacetaldehyde	5.6 ± 0.2	2.0
10	Cyclohexanol	Cyclohexanone	55.7 ± 0.8	19.6
11	2-Hexanol	2-Hexanone	70.7 ± 1.7	24.9
12	Benzyl alcohol	Benzaldehyde	76.9 ± 5.8	27.0
		benzoic acid	trace	—
13	benzyl alcohol/benzyl alcohol- <i>d</i> ₇	$k_{\text{H}}/k_{\text{D}}$	3.1 ± 0.5	—

^a See Experimental section for details. ^b Based on MCPBA. ^c Turnover numbers.

was determined to be 1.7 (entry 8), indicating the preference of *cis*-olefin epoxidation to *trans*-olefin epoxidation by the intermediate generated in the reaction of **6** and MCPBA.

With styrene, the dominant reaction involved the formation of the epoxide, yielding styrene oxide (64.3%) with some amounts of benzaldehyde (11.6%) and phenylacetaldehyde (5.6%; entry 9). Product distribution of this aromatic olefin suggests that either the peroxy radical or oxocobalt(IV) is partly involved as the epoxidizing agent since these species would oxidize *cis*-aromatic olefins to non-stereospecific or radical-induced rearranged products.⁴⁰ In the literature, cobalt(IV)-oxo species⁴¹ and, to a lesser extent, cobalt(V)-oxo species are commonly proposed to be the active intermediates for oxygen transfer in reactions mediated by cobalt compounds with oxidants such as MCPBA and PhIO,⁴² while the reactions of cobalt complexes with hydroperoxides often proceed *via* free-radical type of oxidation reactions.⁴³ Moreover, several groups have proposed a $\text{Co}^{\text{V}}=\text{O}$ intermediate as a reactive species responsible for olefin epoxidation,⁴² whereas a $\text{Co}^{\text{IV}}=\text{O}$ complex was ascribed radical-type oxidations to account for the product distribution in the Co^{III} -catalyzed epoxidation of a radical probe.⁴¹

Therefore, a minimal portion of free radical oxidation reactions, a high degree of stereospecificity, and the formation of some aldehydes from the epoxidation reaction of *cis*-aromatic olefin observed in our catalytic systems imply that two different oxidants, $\text{Co}^{\text{V}}=\text{O}$ and $\text{Co}^{\text{IV}}=\text{O}$, might be produced in these catalytic reactions. We propose that the $\text{Co}^{\text{IV}}=\text{O}$ complex would be responsible for the non-stereoretentive portion of the epoxidation reaction. Importantly, to the best of our knowledge, **6** is the most effective cobalt catalyst that affords high epoxide yields, small amounts of allylic oxidation products, and a high stereospecificity in the epoxidation of olefins by MCPBA.⁴¹⁻⁴³

To obtain more information about the nature of the reactive intermediates we studied the influence of the substituent electronic effects on the rate of epoxidation using styrene and five *para*-substituted styrenes. The rate data gave a good linear Hammett plot against σ^+ with a ρ -value of -0.8 (Fig. S1 in the Supporting Information, SI†). This confirms the expected electrophilic character of the oxidant and the value compares well with those reported for the epoxidation of styrenes using manganese(III) tetraphenylporphyrin ($\rho = -0.41$),⁴⁴ and manganese(III) salen ($\rho = -0.3$)⁴⁵ systems. The latter two systems are believed to involve $\text{Mn}^{\text{V}}=\text{O}$ species as the active oxidant.

Alcohols were also converted efficiently to the corresponding carbonyl compounds (entries 10–12). 2-Hexanol was oxidized to 2-hexanone (70.7%) and benzyl alcohol to benzaldehyde (77%). For solutions containing a low concentration of benzyl alcohol, the product benzaldehyde underwent further oxidation to benzoic acid (data not shown). Kinetic isotope effect (KIE) studies have been used as a mechanistic probe in alkane hydroxylation reactions catalyzed by both iron-containing enzymes and model complexes.⁴⁶ To gain insight into the nature of the oxidizing species in the alcohol oxidation reactions catalyzed by **6**, we performed intermolecular competition reactions involving benzyl alcohol and benzyl alcohol-*d*₇. The kinetic isotope effect for benzaldehyde formation by **6** and MCPBA was determined to be 3.1 ± 0.5 (entry 13), which is nearly identical to that of a hydrogen abstraction reaction catalyzed by a high-valent iron-oxo (3.2 ± 0.3).^{1b} This value strongly indicates that cleavage of the (benzylic) C–H bond is involved in the rate-determining step. Based on this result,

we propose that the reactive species responsible for the alcohol oxidation in our catalytic system might be a similar high-valent cobalt intermediate that is produced following heterolytic O–O bond cleavage of acylperoxy intermediate $\text{Co}-\text{OOC}(\text{O})\text{R}$. In the present study, we report for the first time that a cobalt trimer **6** catalyzes the olefin epoxidation and alcohol oxidation by MCPBA *via* a non-radical type of oxidation reaction, while the structure of the Co catalyst in its active state during the catalysis is not clear yet. Nevertheless, we are speculating that it might be the high-valent Co^{V} -oxo for oxygen atom transfer in the epoxidation reaction. Future studies will focus on attempts to understand the exact nature of the reactive intermediate.

Conclusions

We have prepared a series of monomeric, trimeric, and tetrameric metal complexes from the reaction of metal (Mn, Fe, Co) ions, *N,N*-bis(2-pyridylmethyl)-2-aminoethanol (bpaeOH), and NaSCN/NaN₃ in MeOH: $[\text{Mn}(\text{bpaeOH})(\text{NCS})_2]$ (**1**), $[\text{Mn}(\text{bpaeO})(\text{N}_3)_2]$ (**2**), $[\text{Fe}(\text{bpaeOH})(\text{NCS})_2]$ (**3**), $[\text{Fe}_4(\text{bpaeO})_2(\text{CH}_3\text{O})_2(\text{N}_3)_8]$ (**4**), $[\text{Co}(\text{bpaeOH})(\text{NCS})_2]$ (**5**), and $[\text{Co}_3(\text{bpaeO})_2(\text{NO}_3)(\text{N}_3)_4](\text{NO}_3)$ (**6**). These are characterized by X-ray crystallography and magnetic data. Compounds **1**, **3**, and **5** are isomorphous structures as distorted octahedral geometries. The structure of **2** is similar to that of **1**, however, the oxidation state of **2** is +3 and different to that of **1** (+2). Compound **4** is a zigzag tetranuclear complex possessing high-spin iron(III) ions and shows both ferromagnetic (*via* end-on azide ion) and antiferromagnetic (*via* oxygen atoms of methoxy and hydroxo groups) couplings between the iron(III) ions within the tetranuclear unit. The compound **6** is a mixed-valence trinuclear cobalt complex, $\text{Co}^{\text{III}}(S = 0)-\text{Co}^{\text{II}}(S = 3/2)-\text{Co}^{\text{III}}(S = 0)$ and displays the magnetic moment of a cobalt(II) ion in a high-spin state. In addition, the reactivity study with the complex **6** describes a robust cobalt catalyst that epoxidizes a wide range of olefins and alcohols with modest to excellent yields, and that represents a new class of inexpensive catalysts for epoxidation and alcohol oxidation reactions. Moreover, we have shown for the first time that the cobalt trimer catalyzes a non-radical type of oxidation reactions with MCPBA as an oxidant. We suggest that a high-valent cobalt-oxo complex might be generated as a reactive oxidizing intermediate in the reaction of the cobalt complex and MCPBA.

Acknowledgements

This work was supported by the Korea Research Foundation (KRF) grant funded by the Korea government (MEST) (No. 2009-0073897).

References

- (a) R. G. Hicks, M. T. Lemaire, L. K. Thompson and T. M. Barclay, *J. Am. Chem. Soc.*, 2000, **122**, 8077; (b) T. Wada, K. Tsuge and K. Tanaka, *Inorg. Chem.*, 2001, **40**, 329; (c) C. Benelli and D. Gatteschi, *Chem. Rev.*, 2002, **102**, 2369; (d) A. K. Poulsen, A. Rompel and C. J. McKenzie, *Angew. Chem., Int. Ed.*, 2005, **44**, 6916; (e) I. Zilbermann, E. Maimon, H. Cohen and D. Meyerstein, *Chem. Rev.*, 2005, **105**, 2609; (f) E. Y. Tshuva and S. J. Lippard, *Chem. Rev.*, 2004, **104**, 987; (g) B. Lane and K. Burgess, *Chem. Rev.*, 2003, **103**, 2457; (h) S. H. Lee, J. H. Han, H. Kwak, S. J. Lee, E. Y. Lee, H. J. Kim, J. H. Lee, C. Bae, S. N. Lee, Y. Kim and C. Kim, *Chem.-Eur. J.*, 2007, **13**, 9393.

- 2 (a) S. H. Strauss, *Chem. Rev.*, 1993, **93**, 927; (b) M. D. Lankshear and P. D. Beer, *Acc. Chem. Res.*, 2007, **40**, 657; (c) S. O. Kang, R. A. Begum and K. Bowman-James, *Angew. Chem., Int. Ed.*, 2006, **45**, 7882; (d) J. H. Han, J. W. Shin and K. S. Min, *Bull. Korean Chem. Soc.*, 2009, **30**, 1113.
- 3 J. W. Shin, S. R. Rowthu, B. G. Kim and K. S. Min, *Dalton Trans.*, 2010, **39**, 2765.
- 4 (a) J. T. Groves and I. O. Kady, *Inorg. Chem.*, 1993, **32**, 3868; (b) K. Saatchi and U. O. Häfeli, *Dalton Trans.*, 2007, 4439; (c) K. Suntharalingam, A. J. P. White and R. Vilar, *Inorg. Chem.*, 2010, **49**, 8371.
- 5 (a) F. Li, M. Wang, P. Li, T. Zhang and L. Sun, *Inorg. Chem.*, 2007, **46**, 9364; (b) J. M. Botha, K. Umakoshi, Y. Sasaki and G. J. Lamprecht, *Inorg. Chem.*, 1998, **37**, 1609; (c) M. J. Young, D. Wahnnon, R. C. Hynes and J. Chin, *J. Am. Chem. Soc.*, 1995, **117**, 9441.
- 6 (a) S. Naiya, C. Biswas, M. G. B. Drew, C. J. Gómez-García, J. M. Clemente-Juan and A. Ghosh, *Inorg. Chem.*, 2010, **49**, 6616; (b) J. Ribas, A. Escuer, M. Monfort, R. Vicente, R. Cortés, L. Lezama and T. Rojo, *Coord. Chem. Rev.*, 1999, **193–195**, 1027; (c) E.-Q. Gao, Y.-F. Yue, S.-Q. Bai, Z. He, S.-W. Zhang and C.-H. Yan, *Chem. Mater.*, 2004, **16**, 1590; (d) E. Ruiz, J. Cano, S. Alvarez and P. Alemany, *J. Am. Chem. Soc.*, 1998, **120**, 11122; (e) O. Sengupta and P. S. Mukherjee, *Inorg. Chem.*, 2010, **49**, 8583; (f) O. Sengupta, G. Bappaditya, S. Mukherjee and P. S. Mukherjee, *Dalton Trans.*, 2010, **39**, 7451; (g) K. C. Mondal, M. G. B. Drew and P. S. Mukherjee, *Inorg. Chem.*, 2007, **46**, 5625.
- 7 (a) C. Fukuhara, E. Asato, T. Shimoji, K. Katsura, M. Mori, K. Matsumoto and S. Ooi, *J. Chem. Soc., Dalton Trans.*, 1987, 1305; (b) T. Tanase, S. Tamakoshi, M. Doi, M. Mikuriya, H. Sakurai and S. Yano, *Inorg. Chem.*, 2000, **39**, 692; (c) D. A. Shultz, in *Magnetism - Molecules to Materials*, ed. J. S. Miller and M. Drillon, Wiley-VCH, Mannheim, 2001, vol. 2, p. 281.
- 8 K. S. Min, A. G. DiPasquale, A. L. Rheingold, H. S. White and J. S. Miller, *J. Am. Chem. Soc.*, 2009, **131**, 6229.
- 9 (a) Y.-Y. Niu, B.-L. Wu, X.-L. Guo, Y.-L. Song, X.-C. Liu, H.-Y. Zhang, H.-W. Hou, C.-Y. Niu and S.-W. Ng, *Cryst. Growth Des.*, 2008, **8**, 2393; (b) K. R. Reddy, M. V. Rajasekharan and J.-P. Tuchagues, *Inorg. Chem.*, 1998, **37**, 5978; (c) Y. Y. Niu, H. G. Zheng, H. W. Hou and X. Q. Xin, *Coord. Chem. Rev.*, 2004, **248**, 169.
- 10 (a) P. Atkins, T. Overton, J. Rourke, M. Weller and F. Armstrong, *Inorganic Chemistry*, Oxford University Press, New York, 4th edn, 2006, pp. 459–461; (b) F. G. Martins, J. F. Andrade, A. C. Pimenta, L. M. Lourenço, J. R. M. Castro and V. R. Balbo, *Ecl. Quím., São Paulo*, 2005, **30**, 63.
- 11 J. M. Botha, K. Umakoshi, Y. Sasaki and G. J. Lamprecht, *Inorg. Chem.*, 1998, **37**, 1609.
- 12 E. Bill, 2008, http://ewww.mpi-muelheim.mpg.de/bac/logins/bill/julX_en.php.
- 13 *Saint Plus*, Version 6.02, Bruker Analytical X-ray, Madison, WI, 1999.
- 14 *SADABS*, Version 2.03, Bruker AXS Inc., Madison, WI, 2000.
- 15 G. M. Sheldrick, *Acta Crystallogr., Sect. A: Found. Crystallogr.*, 1990, **46**, 467.
- 16 G. M. Sheldrick, *SHELXL-97, Program for refinement of crystal structures*, University of Göttingen, Germany, 1997.
- 17 A. L. Spek, *J. Appl. Crystallogr.*, 2003, **36**, 7.
- 18 S. H. Lee, L. Xu, B. K. Park, Y. V. Mironov, S. H. Kim, Y. J. Song, C. Kim, Y. Kim and S. J. Kim, *Chem.–Eur. J.*, 2010, **16**, 4678.
- 19 K. Nakamoto, *Infrared and Raman Spectra of Inorganic and Coordination Compounds*, John Wiley and Sons, Inc., New Jersey, 6th edn, 2009, Part B, pp. 120–131.
- 20 H. Oshio, E. Ino, I. Mogi and T. Ito, *Inorg. Chem.*, 1993, **32**, 5697.
- 21 (a) M. U. Triller, D. Pursche, W.-Y. Hsieh, V. L. Pecoraro, A. Rempel and B. Krebs, *Inorg. Chem.*, 2003, **42**, 6274; (b) C. M. Coates, S. R. Fiedler, T. L. McCullough, T. E. Albrecht-Schmitt, M. P. Shores and C. R. Goldsmith, *Inorg. Chem.*, 2010, **49**, 1481.
- 22 (a) G. R. Desiraju, *Crystal Engineering: The Design of Organic Solids*, Elsevier, New York, 1989, ch. 4; (b) A. S. Shetty, J. Zhang and J. S. Moore, *J. Am. Chem. Soc.*, 1996, **118**, 1019; (c) W. B. Jennings, B. M. Farrell and J. F. Malone, *Acc. Chem. Res.*, 2001, **34**, 885.
- 23 (a) G. Aromi, M. J. Knapp, J.-P. Claude, J. C. Huffman, D. N. Hendrickson and G. Christou, *J. Am. Chem. Soc.*, 1999, **121**, 5489; (b) B. Albela, R. Carina, C. Policar, S. Poussereau, J. Cano, J. Guilhem, L. Tchertanov, G. Blondin, M. Delroisse and J.-J. Girerd, *Inorg. Chem.*, 2005, **44**, 6959.
- 24 (a) W. Liu and H. H. Thorp, *Inorg. Chem.*, 1993, **32**, 4102; (b) I. D. Brown and D. Altermatt, *Acta Crystallogr., Sect. B: Struct. Sci.*, 1985, **41**, 244; (c) N. E. Brese and M. O’Keeffe, *Acta Crystallogr., Sect. B: Struct. Sci.*, 1991, **47**, 192; (d) R. M. Wood, K. A. Abboud, R. C. Palenik and G. J. Palenik, *Inorg. Chem.*, 2000, **39**, 2065; (e) J. Zachara, *Inorg. Chem.*, 2007, **46**, 9760.
- 25 J. Simaan, S. Poussereau, G. Blondin, J.-J. Girerd, D. Defaye, C. Philouze, J. Guilhem and L. Tchertanov, *Inorg. Chim. Acta*, 2000, **299**, 221.
- 26 (a) A. Bondi, *J. Phys. Chem.*, 1964, **68**, 441; (b) E. W. Reinheimer, M. Fourmigué and K. R. Dunbar, *J. Chem. Crystallogr.*, 2009, **39**, 723; (c) R. D. Shannon and C. T. Prewitt, *Acta Crystallogr., Sect. B: Struct. Crystallogr. Cryst. Chem.*, 1970, **26**, 1046.
- 27 L. Antolini, A. C. Fabretti, D. Gatteschi, A. Giusti and R. Sessoli, *Inorg. Chem.*, 1991, **30**, 4858.
- 28 B. Albela, R. Carina, C. Policar, S. Poussereau, J. Cano, J. Guilhem, L. Tchertanov, G. Blondin, M. Delroisse and J.-J. Girerd, *Inorg. Chem.*, 2005, **44**, 6959.
- 29 L. R. Gahan, V. A. Grillo, T. W. Hambley, G. R. Hanson, C. J. Hawkins, E. M. Proudfoot, B. Moubaraki, K. S. Murray and D. Wang, *Inorg. Chem.*, 1996, **35**, 1039.
- 30 W. A. Gunderson, A. I. Zatsman, J. P. Emerson, E. R. Farquhar, L. Que Jr., J. D. Lipscomb and M. P. Hendrich, *J. Am. Chem. Soc.*, 2008, **130**, 14465.
- 31 (a) S.-W. Hung, F.-A. Yang, J.-H. Chen, S.-S. Wang and J.-Y. Tung, *Inorg. Chem.*, 2008, **47**, 7202; (b) Q. Scheifele, C. Riplinger, F. Neese, H. Weihe, A.-L. Barra, F. Juranyi, A. Podlesnyak and P. L. W. Tregenna-Piggott, *Inorg. Chem.*, 2008, **47**, 439; (c) G. Aromi, M. J. Knapp, J.-P. Claude, J. C. Huffman, D. N. Hendrickson and G. Christou, *J. Am. Chem. Soc.*, 1999, **121**, 5489; (d) B. Albela, R. Carina, C. Policar, S. Poussereau, J. Cano, J. Guilhem, L. Tchertanov, G. Blondin, M. Delroisse and J.-J. Girerd, *Inorg. Chem.*, 2005, **44**, 6959; (e) J. D. Harvey, C. J. Ziegler, J. Telsler, A. Ozarowski and J. Krzystek, *Inorg. Chem.*, 2005, **44**, 4451.
- 32 A. Ozarowski, S. A. Zvyagin, W. M. Reiff, J. Telsler, L.-C. Brunel and J. Krzystek, *J. Am. Chem. Soc.*, 2004, **126**, 6574.
- 33 (a) L. Borer, L. Thalken, C. Ceccarelli, M. Glick, J. H. Zhang and W. M. Reiff, *Inorg. Chem.*, 1983, **22**, 1719; (b) D. M. Kurtz, *Chem. Rev.*, 1990, **90**, 585.
- 34 G. De Munno, T. Poerio, G. Viau, M. Julve and F. Lloret, *Angew. Chem., Int. Ed. Engl.*, 1997, **36**, 1459.
- 35 J. M. Clemente-Juan, C. Mackiewicz, M. Verelst, F. Dahan, A. Bousseksou, Y. Sanakis and J.-P. Tuchagues, *Inorg. Chem.*, 2002, **41**, 1478.
- 36 (a) D. M. Duggan and D. N. Hendrickson, *Inorg. Chem.*, 1975, **14**, 1944; (b) O. Kahn, *Molecular Magnetism*, VCH, New York, 1993, p. 38.
- 37 (a) B. J. Kennedy, G. D. Fallon, B. M. K. C. Gatehouse and K. S. Murray, *Inorg. Chem.*, 1984, **23**, 580; (b) R. W. Handel, H. Willms, G. B. Jameson, K. J. Berry, B. Moubaraki, K. S. Murray and S. Brooker, *Eur. J. Inorg. Chem.*, 2010, 3317; (c) J. Krzystek, S. A. Zvyagin, A. Ozarowski, A. T. Fiedler, T. C. Brunold and J. Telsler, *J. Am. Chem. Soc.*, 2004, **126**, 2148.
- 38 (a) T. Punniyamurthy, S. Velusamy and J. Iqbal, *Chem. Rev.*, 2005, **105**, 2329; (b) M. Costas, M. P. Mehn, M. P. Jensen and L. Que Jr., *Chem. Rev.*, 2004, **104**, 939.
- 39 T. K. M. Shing, Y. Y. Yeung and P. L. Su, *Org. Lett.*, 2006, **8**, 3149.
- 40 (a) F. A. Chavez, J. A. Briones, M. M. Olmstead and P. K. Mascharak, *Inorg. Chem.*, 1999, **38**, 1603; (b) F. A. Chavez and P. K. Mascharak, *Acc. Chem. Res.*, 2000, **33**, 539; (c) N. S. Sehlotho and T. Nyokong, *J. Mol. Catal. A: Chem.*, 2004, **209**, 51; (d) J. T. Groves and M. K. Stern, *J. Am. Chem. Soc.*, 1988, **110**, 8628; (e) J. T. Groves and M. K. Stern, *J. Am. Chem. Soc.*, 1987, **109**, 3812.
- 41 (a) T. Punniyamurthy, B. Bhatia, M. M. Reddy, G. C. Maikap and J. Iqbal, *Tetrahedron*, 1997, **53**, 7649; (b) T. Punniyamurthy, S. J. S. Kalra and J. Iqbal, *Tetrahedron Lett.*, 1995, **36**, 8497; (c) L. Saussine, E. Brazi, A. Robine, H. Mimoun, J. Fisher and R. Weiss, *J. Am. Chem. Soc.*, 1985, **107**, 3534; (d) D. Dhar, Y. Kolytipin, A. Gedanken and S. Chandrasekaran, *Catal. Lett.*, 2003, **86**, 197; (e) I. Fernandez, J. R. Pedro, A. L. Rosello, R. Ruiz, I. Castro, X. Ottenwaelder and Y. Journaux, *Eur. J. Org. Chem.*, 2001, 1235; (f) J. D. Koola and J. K. Kochi, *J. Org. Chem.*, 1987, **52**, 4545.
- 42 (a) D. Mansuy, J.-F. Bartoli and M. Momenteau, *Tetrahedron Lett.*, 1982, **23**, 2781; (b) W. A. Lee and T. C. Bruce, *Inorg. Chem.*, 1986, **25**, 131; (c) T. J. Collins, S. Ozaki and T. G. Richmond, *J. Chem. Soc., Chem. Commun.*, 1987, 803; (d) W. Nam, I. Kim, Y. Kim and C. Kim,

- Chem. Commun.*, 2001, 1262; (e) W. Nam, J. Y. Ryu, I. Kim and C. Kim, *Tetrahedron Lett.*, 2002, **43**, 5487.
- 43 (a) F. A. Chavez, J. M. Rowland, M. M. Olmstead and P. K. Mascharak, *J. Am. Chem. Soc.*, 1998, **120**, 9015; (b) S. Forster and A. Rieker, *J. Org. Chem.*, 1996, **61**, 3320; (c) F. A. Chavez, C. V. Nguyen, M. M. Olmstead and P. K. Mascharak, *Inorg. Chem.*, 1996, **35**, 6282.
- 44 O. Bortolini and B. Meunier, *J. Chem. Soc., Perkin Trans. 2*, 1984, 1967.
- 45 (a) K. Srinivasan, P. Michaud and J. K. Kochi, *J. Am. Chem. Soc.*, 1986, **108**, 2309; (b) W. Adam, C. Mock-Knoblach, C. R. Saha-Moller and M. Herderich, *J. Am. Chem. Soc.*, 2000, **122**, 9685.
- 46 (a) A. Sorokin, A. Robert and B. Meunier, *J. Am. Chem. Soc.*, 1993, **115**, 7293; (b) J. I. Manchester, J. P. Dinnocenzo, L. Higgins and J. P. Jones, *J. Am. Chem. Soc.*, 1997, **119**, 5069; (c) M. Newcomb, D. Aebisher, R. Shen, R. E. P. Chandrasena, P. F. Hollenberg and M. J. Coon, *J. Am. Chem. Soc.*, 2003, **125**, 6064; (d) J. H. Han, S.-K. Yoo, J. S. Seo, S. J. Hong, S. K. Kim and C. Kim, *Dalton Trans.*, 2005, 402.